Open Channel Block and Alteration of *N*-Methyl-D-Aspartic Acid Receptor Gating by an Analog of Phencyclidine

J. G. Dilmore and J. W. Johnson
Department of Neuroscience, University of Pittsburgh, Pittsburgh, Pennsylvania 15260 USA

ABSTRACT   We investigated inhibition of the *N*-methyl-D-aspartic acid (NMDA) receptor-channel complex by *N*-ethyl-1,4,9,9α-tetrahydro-4αR-cis-4αH-fluoren-4α-amine (NEFA), a structural analog of phencyclidine (PCP). Using the whole-cell recording technique, we demonstrated that NEFA inhibits NMDA responses with an IC$_{50}$ of 0.51 μM at -66 mV. We determined that NEFA binds to the open channel, and subsequently the channel can close and trap the blocker. Once the channel has closed, NEFA is unable to dissociate until the channel reopens. Single-channel recordings revealed that NEFA reduces the mean open time of single NMDA-activated channels in a concentration-dependent manner with a forward blocking rate (k_{+}) of 39.9 μM^{-1} s^{-1}. A computational model of antagonism by NEFA was developed and constrained using kinetic measurements of single-channel data. By multiple criteria, only models in which blocker binding in the channel causes a change in receptor operation adequately fit or predicted whole-cell data. By comparing model predictions and experimental measurements of NEFA action at a high NMDA concentration, we determined that NEFA affects receptor operation through an influence on channel gating. We conclude that inhibition of NMDA receptors by PCP-like blockers involves a modification of channel gating as well as block of current flow through the open channel.

INTRODUCTION

N-methyl-D-aspartic acid (NMDA) receptors have been the focus of extensive study due in part to their demonstrated roles in such physiological processes as synapse formation during development and long term changes in synaptic efficacy. NMDA receptors have attracted attention also because their overactivation has been implicated in a variety of pathological conditions including ischemia (Rothman and Olney, 1995) and epilepsy (Rogawski, 1993). There has been extensive research into the possibility that the deleterious consequences of NMDA receptor overactivation may be prevented or reduced by the use of antagonists of NMDA receptor function. One mechanism by which potentially therapeutic antagonists could act is by blocking the channel of the NMDA receptor.

Numerous drugs have been found that block the channel of the NMDA receptor with high affinity, but their therapeutic potential varies tremendously. MK-801, ketamine, and phencyclidine (PCP) are three such compounds (Huettner and Bean, 1988; Mayer et al., 1988; MacDonald et al., 1991) that appear to have limited therapeutic value. PCP and ketamine have unacceptable psychotomimetic effects in humans (Luby et al., 1959; Krystal et al., 1994), and behavioral studies in a variety of species suggest that MK-801 has similar psychotomimetic effects (reviewed in Ellison, 1995). In contrast, other NMDA receptor channel blockers,

such as memantine and amantadine, are routinely used in the treatment of neurodegenerative diseases including Parkinson's disease (Fischer et al., 1997) and are well tolerated clinically (Ditzler, 1991). Several experimenters have proposed that the mechanism of action of an antagonist plays a crucial role in determining its therapeutic potential in the treatment of the pathological conditions (Chen et al., 1992; Rogawski, 1993; Antonov et al., 1995; Blanpied et al., 1997). A thorough understanding of the interaction between channel blockers and NMDA receptors would clearly advance the prospects of designing new NMDA antagonists for therapeutic use.

The classical description of open channel block, based on block of nicotinic acetylcholine receptors by local anesthetics, utilized the sequential model (Adams, 1976; Neher and Steinbach, 1978). In this model, the antagonist can bind only to open channels and its presence in the channel prevents channel closure as well as current flow though the channel. Several drugs have been proposed to act as sequential blockers of the NMDA receptor channel including 9-aminoacridine (Costa and Albuquerque, 1994; Benveniste and Mayer, 1996) and IEM-1857 (Antonov and Johnson, 1996).

PCP (Lerma et al., 1991; MacDonald et al., 1991), MK-801 (Huettner and Bean, 1988), ketamine (MacDonald et al., 1991), and memantine (Blanpied et al., 1997; Chen and Lipton, 1997) have been shown to inhibit NMDA responses by the related "trapping" model of open channel block. As in the sequential scheme, the antagonist has access to its binding site only when the channel is open. In contrast to sequential blockers, trapping blockers permit channel closure while they are bound. Following channel closure, the agonists can unbind, trapping the blocker within the closed channel. We have used the following scheme (see Methods)
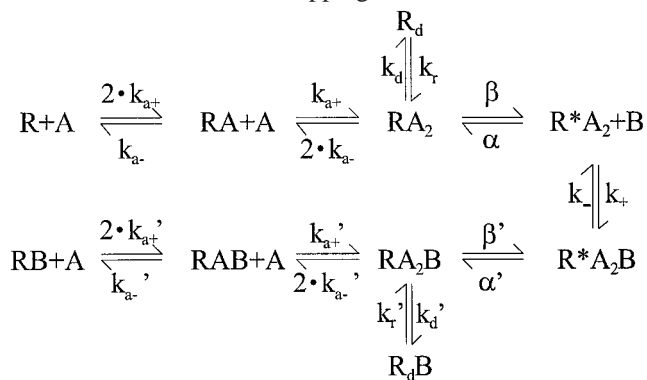
to describe the action of trapping channel blockers:

$$R+A \underset{k_{a-}}{\overset{2 \cdot k_{a+}}{\rightleftharpoons}} RA+A \underset{2 \cdot k_{a-}}{\overset{k_{a+}}{\rightleftharpoons}} RA_2 \underset{\alpha}{\overset{\beta}{\rightleftharpoons}} R^*A_2+B$$

with R_d above RA_2 connected by $k_d \Vert k_r$, and R^*A_2+B connected to R^*A_2B by $k_- \Vert k_+$:

$$RB+A \underset{k_{a-}'}{\overset{2 \cdot k_{a+}'}{\rightleftharpoons}} RAB+A \underset{2 \cdot k_{a-}'}{\overset{k_{a+}'}{\rightleftharpoons}} RA_2B \underset{\alpha'}{\overset{\beta'}{\rightleftharpoons}} R^*A_2B$$

with R_dB below RA_2B connected by $k_r' \Vert k_d'$.

Scheme 1

where R is the NMDA receptor, A is NMDA, B is the blocker, an asterisk indicates that the channel is open, and R_d is the desensitized state of the receptor. The model may be conceptualized as having two partitions, an upper arm that does not have blocker bound, and a lower arm that does, connected by the blocker binding and unbinding reactions. The rates of transitions among the states in the lower arm of the model have a great influence on the inhibitory effects of a trapping blocker (Lingle, 1983; Johnson et al., 1995). It is sometimes assumed that binding of a trapping blocker does not influence receptor operation (that is, that corresponding rates of transitions in the upper and lower arms of trapping block models are the same; e.g., Huettner and Bean, 1988; MacDonald et al., 1991), but the validity of this assumption has not been examined. Differences between the rates of transitions in the upper and lower arms have been proposed to explain some of the actions of memantine and amantadine (Blanpied et al., 1997; Chen and Lipton, 1997). A central goal of this article is to determine whether binding of PCP-like blockers influences receptor operation.

Because PCP is strongly psychotomimetic, a detailed understanding of its mechanism of action may provide insight into the properties that determine whether an NMDA receptor channel blocker can be used clinically. Unfortunately, electrophysiological investigations of the action of PCP are difficult to perform due to its slow kinetics (MacDonald et al., 1991). We have overcome this limitation by analyzing the actions of one of the conformationally restricted structural analogs of PCP synthesized by Kozikowski and Pang (1990), N-ethyl-1,4,9,9α-tetrahydro-4αR-cis-4αH-fluoren-4α-amine (NEFA; Fig. 1). NEFA was shown to displace [³H]MK-801 with lower affinity than PCP. We therefore expected that it would exhibit faster kinetics than PCP, permitting us to examine and model its mechanism of action over a range of concentrations. NEFA provides an easily manipulated experimental model for the interactions of PCP with the NMDA-receptor channel complex.

We have characterized NEFA using whole-cell and single-channel patch clamp techniques and found it to be an intermediate-affinity trapping open channel blocker of the
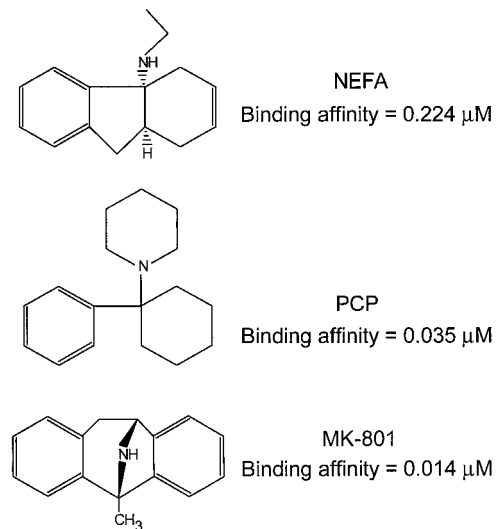

FIGURE 1   The chemical structures of NEFA, PCP, and MK-801. The binding affinities are taken from Kozikowski and Pang (1990) and were determined by displacement of [³H]MK-801.

NMDA receptor. Computational modeling of the antagonism suggests that, when bound in the channel, NEFA influences receptor operation through an effect on channel gating. Some of the data in this paper have been previously presented in abstract form (Dilmore and Johnson, 1994, 1995).

METHODS

Cell culture

Forebrain cultures were prepared as described in Antonov et al. (1995). Briefly, pregnant Sprague-Dawley rats were sacrificed at 16 days after conception by CO_2 inhalation and the cerebral hemispheres of the embryos were removed. The hemispheres were dissociated and cells were plated at a density of approximately 2×10^5 cells/ml onto a poly-L-lysine-coated glass coverslip and grown in a serum-containing medium.

Whole-cell recording

The whole-cell configuration of the patch-clamp recording technique was used to record current from the cultured rat neurons three to six weeks after plating. The intracellular solution contained 120 or 100 mM CsF, 10 mM CsCl, 10 mM HEPES, and 10 mM 1,2-bis-(2-aminophenoxy)ethane-N,N,N',N'-tetraacetic acid (BAPTA). The pH was adjusted to 7.2 by adding CsOH. Pipettes were pulled from thin wall borosilicate glass (o.d. 1.5 mm; i.d. 1.17 mm, Warner Instruments Corp., Hamden, CT) that contained a thin filament. Pipette resistances were between 1.5 and 5 MΩ and series resistance compensation was used in many experiments. The extracellular solutions consisted of a stock solution of drug dissolved in control solution. Control solution contained 140 mM NaCl, 2.8 mM KCl, 0.4 or 1.0 mM $CaCl_2$, and 10 mM HEPES. Cells were initially bathed in this 1 mM $CaCl_2$ control solution while a gigaohm seal was made. After rupture of the patch of membrane the extracellular solution was changed to control solution containing 0.4 mM calcium. Intracellular BAPTA and low extracellular calcium were used to reduce calcium dependent inactivation of the NMDA response (Rosenmund and Westbrook, 1994). Unless otherwise noted, a concentration of 5 μM NMDA was used to activate responses. In all experiments, 10 μM glycine was coapplied with NMDA. Both 200 nM

tetrodotoxin and 1 μM strychnine were included in all extracellular solutions to inhibit spontaneous synaptic inputs and activation of inhibitory glycine receptors, respectively. Stock solutions were kept frozen until the day of experimentation. All voltages are corrected for the -6-mV junction potential that was measured between the intracellular and extracellular solutions. All chemicals were purchased from Sigma Chemicals (St. Louis, MO) except for NEFA, which was the generous gift of Drs. Alan Kozikowski and Yuan-Ping Pang.

The extracellular solutions were controlled by using a five-barrel fast perfusion system (Blanpied et al., 1997; see "Computational modeling" below). The barrels were placed approximately 100 μm from the cell under study. Whole-cell current traces were filtered at 5 Hz using a Butterworth lowpass filter and sampled at 20 Hz using the Fetchex module of PCLAMP 6.02 software (Axon Instruments, Foster City, CA). Single exponential functions were fit to the slow phase of onset and offset of inhibition using PCLAMP's Clampfit module and the SIMPLEX method of error minimization. The time constant of recovery from inhibition was measured by fitting a single exponential function to the whole-cell current during the first 75 s of agonist application following removal of antagonists as described in the text. The concentration-inhibition curve was constructed by fitting whole-cell current data measured at -66 mV with the following equation:

$$\frac{I_{\text{NMDA}} - I_{\text{B}}}{I_{\text{NMDA}}} = \frac{1}{1 + \left(\frac{\text{IC}_{50}}{[\text{B}]}\right)^{n_{\text{H}}}} \qquad (1)$$

where I_{NMDA} = steady state current invoked by NMDA + glycine application, I_{B} = steady state current in the presence of NEFA and agonist solution, IC_{50} = concentration (in μM) where 50% of the response is inhibited, [B] = blocker concentration (μM), and n_{H} is the Hill coefficient, which reflects cooperativity of drug action. In all concentration-inhibition plots, percent inhibition is plotted on the ordinate.

The voltage dependence of antagonism was determined by fitting whole-cell current data measured over a range of membrane potentials with the following equation:

$$\frac{I_{\text{B}}}{I_{\text{NMDA}}} = \frac{1}{1 + \frac{[\text{B}]}{K_0 e^{V_{\text{m}}/V_0}}} \qquad (2)$$

where [B] is blocker concentration (μM), K_0 is the IC_{50} (μM) for the blocker at 0 mV, V_{m} is the membrane voltage (in mV), and V_0 is the change in V_{m} that results in an e-fold change in IC_{50}.

Single-channel recording

The outside-out configuration of the patch-clamp technique (Hamill et al., 1981) was used to record single-channel currents. The intracellular and extracellular solutions were the same as those used in whole-cell recording. In all single-channel experiments, solutions containing 10 μM NMDA + 10 μM glycine were used to activate NMDA receptors. Pipettes were pulled from standard wall borosilicate glass (o.d. 1.5 mm; i.d. 0.86 mm) that contained a thin filament; their resistance ranged from 7 to 12 MΩ. The data were filtered at 2 kHz (f_c) using an 8-pole Bessel filter and sampled at 20 kHz using the Fetchex module of PCLAMP 6.02 software. Transitions between the closed and open states were identified using half amplitude event detection (Colquhoun and Sigworth, 1995). The data from a patch were rejected if >5% of all channel openings were multiple level openings. Data for open time analysis included patches that contained 203 to 3910 channel openings (mean, 914 $\pm$ 229). Closed time analysis was performed on patches that displayed from 596 to 2962 channel closures (mean, 1542 $\pm$ 468). Histograms were plotted as the logarithm of event duration *versus* the square root of the number of events (Sigworth and Sine, 1987). Histograms were fitted with exponential functions by the log maximum likelihood method (Colquhoun and Sigworth, 1995) using the PStat

module of PCLAMP 6.02 software. The majority (16/18) of open time distributions were fitted with two exponentials; the remainder were adequately fitted with a single exponential. Closed and open times shorter than 0.181 ms (approximately $2 \cdot 0.179/f_c$; Colquhoun and Sigworth, 1995) were deleted from histograms before fitting, and the fits were corrected for the deleted events. No attempt to correct open times for missed closures or closed times for missed openings was made. The consistency of the data presented here with previous recordings at higher time resolutions where corrections were made (e.g., Antonov and Johnson, 1996) suggest that no significant errors were introduced.

Burst analysis was performed to estimate the channel closing rate (α in Scheme 1). If the NMDA receptor had a single open state accessible from only one fully liganded closed state, then α could be estimated as the inverse of the mean open time. However, the complex behavior of the NMDA receptor (e.g., Gibb and Colquhoun, 1992; Kleckner and Palotta, 1995) resulted in two complications in estimating α. First is a population of brief openings. To approximate as accurately as possible the activity of NMDA receptors with the simplified model of Scheme 1, we ignored the brief open time, in which the NMDA receptor spends far less time than in the main open state (see Fig. 6). A second complication is the presence of multiple closed-time populations, three of which were resolved here (see Results). The state occupied during the briefest population of closures may have access only to the open state (Jahr and Stevens, 1990), and is occupied far less than the open state (Antonov and Johnson, 1996). The briefest closed state thus has little effect on total current flow, and we ignored it in estimating α. The duration of the longest closed state depends on agonist concentration (Antonov and Johnson, 1996), suggesting that entry into this state involves agonist unbinding. We therefore defined transitions to the briefest closed state as within-burst and transitions to the intermediate and longest closed states as between-burst. We estimated α as the inverse of the mean burst duration, which approximates the rate of entry into the first significantly occupied closed state accessible from the main open state. The approximately 40-fold separation between the time constants of the briefest and intermediate closed times permitted a reasonably unambiguous definition of bursts. The critical time used to define bursts (t_{crit}) was defined so that the number of short events misclassified as between bursts and the number of long events misclassified as within bursts were equal (Method 2 from Colquhoun and Sigworth, 1995). The values of t_{crit} ranged from 1.03 to 2.58 ms, with an average of 1.93 $\pm$ 0.22 ms; these values are consistent with previous measurements (e.g., Howe et al., 1988; Traynelis and Cull-Candy, 1991; Gibb and Colquhoun, 1992; Antonov and Johnson, 1996). The mean burst duration for each patch was calculated as the arithmetic mean of burst durations.

Computational modeling

Whole-cell current during application of agonists and NEFA were fitted with Scheme 1. The upper arm of Scheme 1 has been reported in numerous studies to model NMDA receptor-mediated whole-cell currents accurately (Clements et al., 1992; Clements and Westbrook, 1991, 1994; Lester and Jahr, 1992; Costa and Albuquerque, 1994; Colquhoun and Hawkes, 1995; Rosenmund et al., 1995). Inclusion of two identical binding sites for NMDA was based on the work of Benveniste and Mayer (1991) and Clements and Westbrook (1991, 1994). Inclusion of glycine binding and allosteric interaction between the glycine and NMDA binding sites (Vyklický et al., 1990) was obviated by addition to all solutions of a nearly saturating concentration (10 μM) of glycine. Interference from Ca^{2+}-dependent desensitization of NMDA receptors (Mayer et al., 1987) was minimized by use of a low extracellular Ca^{2+} concentration (0.4 mM) and inclusion of BAPTA in the intracellular solution. Under these conditions, desensitization is well modeled by a single desensitized state accessible only from the fully liganded closed receptor (Clements and Westbrook, 1991; Lester and Jahr, 1992; Lester et al., 1993). The inclusion of a desensitization step from the open state (Lin and Stevens, 1994) was shown to be unnecessary (Colquhoun and Hawkes, 1995). The specific form of Scheme 1 used to model channel block was adapted from previous studies (Neher, 1982; Lingle, 1983; Huettner and Bean, 1988; MacDonald et al.,

TABLE 1   Values for rate constants determined by fitting the No Effect, Gating, and Binding models to whole-cell current traces

Model	k_- (s^{-1})	k'_{a+} (μM^{-1} s^{-1})	k'_{a-} (s^{-1})	α' (s^{-1})	β' (s^{-1})
No Effect	6.9 ± 1.35	2.1*	22.9*	121*	3.1*
Gating	90.3 ± 19	2.1*	22.9*	41.4 ± 4.6	0.23 ± 0.06
Binding	227 ± 30	0.59 ± 0.36	30.6 ± 15	121*	3.1*

* Values that were held constant during fitting. The other values in the table are means of five measurements $\pm$ SE. The remaining rate constants in Scheme 1 were held constant during fitting of all three models. Two such rate constants were determined from single channel data presented here: $\alpha = 121$ s^{-1}; $k_+ = 39.9$ μM^{-1} s^{-1}. Values for the other rate constants were set based on previously published data (see Methods): $k_{a+} = 2.1$ μM^{-1} s^{-1}; $k_{a-} = 22.9$ s^{-1}; $\beta = 3.1$ s^{-1}; $k_d = k'_d = 5$ s^{-1}; $k_r = k'_r = 1$ s^{-1}. The number of channels, a parameter used to scale the size of the response, was free in all fits.

1991; Costa and Albuquerque, 1994; Chen and Lipton, 1997; Blanpied et al., 1997).

All the rate constants in the upper arm of Scheme 1 were fixed during computational modeling (see Table 1 for values). The agonist binding and unbinding rates were taken from Benveniste and Mayer (1991). The channel closing rate, α, was estimated from burst analysis performed here. The channel opening rate, β, was calculated from the value of α and the maximal probability of a channel being open (maximal $P_{open} = 0.025$; Rosenmund et al., 1995) based on the equation $\beta/(\alpha+\beta) = $ maximal P_{open}. We used the value of maximal P_{open} that Rosenmund et al. (1995) estimated from the charge transfer measurements during whole-cell recordings in the presence of MK-801 and agonists. The result of this approach was preferred because it required the fewest assumptions regarding the mechanism of action of MK-801. The value of the resensitization rate (k_r) was based on the measurements of Lester et al. (1993) and Sather et al. (1992). The value of the desensitization rate (k_d) was set to the value reported by Lester et al. (1993). This value was somewhat arbitrary, given the wide range of desensitization rates that were observed in our experiments. However, data fitting and simulations were also performed with a model that did not contain a desensitized state and similar results were obtained (data not shown). Fitting inaccuracies due to cell-to-cell variability in desensitization kinetics were minimized by the use of a low concentration (5 μM) of NMDA.

Simulations of whole-cell current during application of agonists and NEFA were performed using SCoP 3.5 (Simulation Resources, Inc., Berrien Springs, MI). The simulations were generated by numerically solving the differential equations that arise from Scheme 1. The model was fitted to whole-cell current traces using the SCoPfit module of SCoP. During fitting runs, rate constants were allowed to vary as described in the text. The χ^2 statistic was used to evaluate goodness of fit. The concentration of drugs rose and fell in the simulations according to an exponential function with a time constant of 40 ms. This is a conservative estimate based on the previous measurement of a 50- to 500-fold replacement of the extracellular solution in 120 ms (Blanpied et al., 1997).

All values are reported as the mean $\pm$ SE. Significance was tested by using one way repeated-measure analyses of variance and two-tailed Student's t-tests where appropriate. The Bonferroni post-hoc correction for multiple comparisons was employed to maintain the family-wise α at 0.05.

RESULTS

Whole-cell recording

Previous work by Kozikowski and Pang (1990) demonstrated that NEFA displaced tritiated MK-801 with an affinity of 224 ± 5 nM (Fig. 1), suggesting that NEFA is an antagonist of the NMDA-activated channel. Initial experiments were performed to test this conclusion electrophysiologically. Fig. 2 A shows an example of the protocol used to measure the whole-cell IC$_{50}$. The voltage of the neuron under study was clamped at -66 mV, 5 μM NMDA and 10 μM glycine were applied for approximately 30 s, and the response was allowed to reach steady state. Blocker was

then applied during continued application of agonists. After response inhibition reached steady state, the antagonist solution was washed off with a solution that contained agonists alone. Percent inhibition was quantified as $100 \cdot (I_{NMDA} - I_B)/I_{NMDA}$, where I_{NMDA} is the steady state current in agonists alone and I_B is the steady state current in the presence of blocker (see Methods). A concentration-inhibition curve is presented in Fig. 2 B. NEFA is a potent inhibitor of NMDA responses with an IC$_{50}$ of 0.51 μM at -66 mV and a Hill coefficient of 1.24.

We next investigated the dependence of the macroscopic kinetics of inhibition on blocker concentration. To ensure that kinetic measurements were made after complete solution exchange, we did not use the first 250 ms of the current
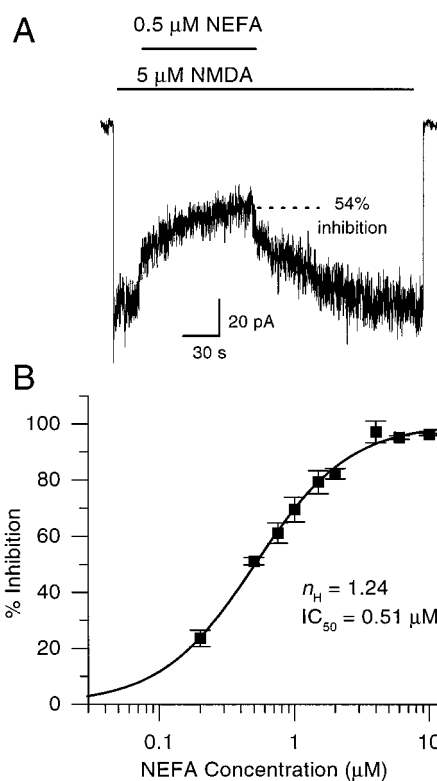

FIGURE 2 NEFA antagonizes the response to NMDA. (A) A current trace from a whole-cell voltage clamp recording is shown. In this and all subsequent figures, NMDA was coapplied with 10 μM glycine. The cell was held at -66 mV. (B) A concentration-inhibition curve was constructed by fitting experimental data with Eq. 1. Each data point represents the mean of measurements from three to six neurons.

record following initiation of solution exchange. As a result, fast components of block that were clear following application of blocker at higher concentrations (Fig. 3 *A*) were ignored. The fast components were typically much smaller than a slower component of block that was reasonably well fitted by a single exponential (Fig. 3 *A*). We used the τ of single exponential fits to the slow component of current relaxations to characterize the macroscopic kinetics of block with a single parameter and to compare our results with previous work. An example of single exponential fits to the onset (time constant τ_{on}) and offset (time constant τ_{off}) of inhibition are shown in Fig. 3 *A*. The inverse of the time constants derived from such fits is plotted as a function of
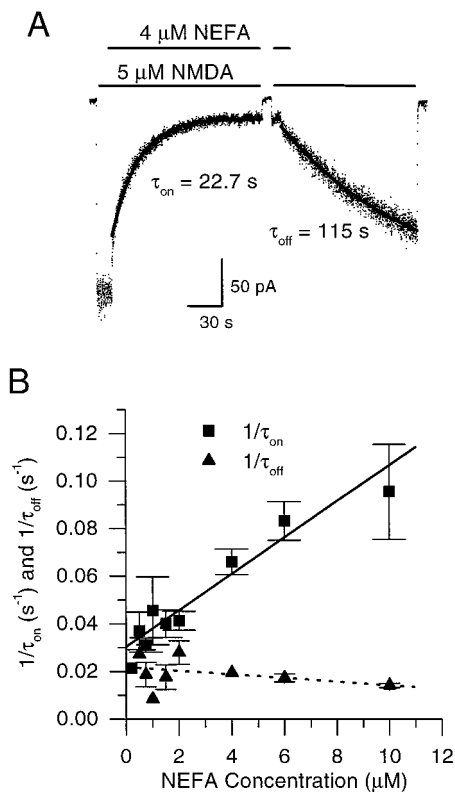

FIGURE 3   Dependence on NEFA concentration of the inverse of the time constants of response inhibition. (*A*) A current trace from a whole-cell recording is shown. The onset and offset of antagonism of whole-cell recordings were fit with single exponential functions (*solid lines*), whose time constants are shown. Fits began 250 ms after the beginning of solution exchange. The cell was held at −66 mV. A brief return to control solution during steady state inhibition as shown here was used to permit accurate determination of baseline current. (*B*) The inverse of the time constant of the single exponential fits to whole-cell current during inhibition by NEFA ($1/\tau_{on}$) is plotted against concentration of NEFA. The data were fit with a straight line and were significantly correlated with the concentration of NEFA ($P < 0.001$). The slope of the line is 0.0076 μM^{-1} s^{-1} and the intercept is 0.03 s^{-1}. The inverse of the time constant of single exponential fits to whole-cell current during recovery from inhibition by NEFA ($1/\tau_{off}$) is plotted against concentration of NEFA. The data were fit with a straight line, and were not significantly correlated with the concentration of NEFA ($P > 0.1$). All data are plotted as means ± SE. Where the number of data points at a given concentration was one or two, the value or mean value is plotted and no error bars are shown.

blocker concentration in Fig. 3 *B*. The inverse of τ_{on} was significantly correlated with concentration (Fig. 3 *B*; $P < 0.001$), indicating that at higher concentrations of NEFA the inhibition proceeded more quickly. The values of the slope and *y*-intercept of this plot are given in Table 2. The inverse of τ_{off} did not correlate with blocker concentration (Fig. 3 *B*; $P > 0.1$). The mean value of τ_{off} was 68 ± 6.7 s.

The voltage dependence of antagonism was also investigated in seven cells at membrane potentials from −66 to +34 mV. The block was strongly voltage dependent, with a 27.2 mV change in voltage producing an *e*-fold difference in IC_{50} (data not shown). This degree of voltage dependence corresponds to a δ (apparent depth in voltage field of binding site) of 0.94 (Woodhull, 1973). This value suggests that the binding site for NEFA is close to the intracellular mouth of the channel. This estimate must be viewed with caution, however, as it has proven to be inaccurate in the case of channel block by Mg^{2+} (Johnson and Ascher, 1990).

We next tested the hypothesis that NEFA behaved according to the trapping model of open channel block. The first set of experiments was performed to determine whether the NMDA receptor could trap NEFA. An experimental paradigm for testing whether an antagonist can be trapped is shown in Fig. 4. It is similar to the protocol shown in Fig. 2 *A* except that when the level of inhibition reached steady state, agonists and antagonist were simultaneously removed, the cell was perfused for 100 s with control solution, and agonists were reapplied without antagonist. If the channel does not trap NEFA, then the response should recover during the 100-s wash in control solution at the same rate as it does in the presence of agonist. Because the τ_{off} in the presence of agonists is 68 ± 6.7 s (Fig. 3 *B*), in 100 s the response should recover to approximately 77% of its original size if NEFA is not trapped. However, if the blocker can be trapped, i.e., if channels accumulate in state RB (Scheme 1) during application of antagonist + agonists, then the response would still be largely antagonized upon reapplication of agonists. Percent trap was quantified as the percent of the original response to NMDA + glycine (measured at steady state just before application of antagonist) that was antagonized upon reapplication of agonists. As shown in Fig. 4 *A*, the initial response evoked by reapplication of agonists was considerably reduced (88%) compared with the control response. This experiment strongly supports the hypothesis that NEFA can be trapped within the closed channel.

An alternative explanation may be presented to account for the apparent trapping. The NMDA channel may close on NEFA and not trap it, but rather slow its unbinding rate. In terms of Scheme 1, channels could accumulate in state RB and slowly "leak" to state R by unbinding of antagonist (transition not shown). It would then appear that NEFA was trapped while in fact it was unbinding very slowly in the absence of agonists. This possibility was tested by varying from 10 to 300 s the duration of the exposure to control solution between the removal of antagonist + agonists and reapplication of agonists. Fig. 4 *B* provides two specific

TABLE 2 Experimentally measured properties of inhibition by NEFA using 5 μM NMDA compared to predictions of the No Effect, Gating, and Binding models

Property	Figure	Experimental data	No Effect model	Gating model	Binding model
IC$_{50}$ (μM)	8 A	0.51	0.16	0.41	0.42
n_H	8 A	1.24	0.98	1	1
Slope (μM^{-1} s^{-1})	8 B	0.0076	0.014	0.0096	0.0097
y-intercept (s^{-1})	8 B	0.030	0.033	0.0169	0.0168
τ_{off}(s)	Not plotted	65.9 $\pm$ 8.7	106 $\pm$ 15.5	115 $\pm$ 16.4	116 $\pm$ 16.4
τ_{on} (s)	8 C	10.2	7.8	12.6	12.6
Steady state inhibition (%)	8 C	96	97.3	93.5	93.4
τ of trap (s)	8 D	13	8.0	12.6	12.8
Steady state trap (%)	8 D	86	89.8	86.7	87.6

Graphical comparisons of experimental values and model predictions are shown in the indicated figures. Model predictions were based on measurements from simulations of the kinetics and steady state level of inhibition of whole-cell currents and of the progression of receptors into the trapped state (see text). The values of τ_{on}, steady state inhibition, τ for trap, and steady state trap were measured using 6 μM NEFA in simulations and in experimental data. To determine the value of τ_{off} for simulations and experimental data, the values of the time constant of recovery from inhibition by each concentration of NEFA were averaged.

examples of the protocol used to test this hypothesis. The two traces show whole-cell current during reapplication of agonists after washes of 10 and 150 s in the same cell. The current traces during reapplication of agonists overlay almost exactly, indicating that NEFA either is unable to unbind from the closed channel or can do so only extremely slowly. Fig. 4 C shows the effect of varying the duration of wash by control solution on the percent of the original response antagonized immediately following reapplication of agonists. The slope of the line was not significantly different from 0 ($P > 0.65$), indicating that the duration of the wash does not significantly affect the percent trap over the duration of recordings obtained in this study. However, the slope of the line that describes the relationship is non-zero (-0.0082%/s), suggesting that unblocking may occur at a very slow rate. Fitting the data in Fig. 4 B with a single exponential decay equation yields a time constant of 2.7 hours. Therefore, determining whether the data in Fig. 4 B reflect very slow unblocking in the absence of agonist (a process that could be important when channel-blocking drugs are used *in vivo*) would require an experimental duration on the hour time scale. When applied alone (i.e., without agonists present), even in high concentrations (40 μM) NEFA does not antagonize subsequent responses to NMDA ($n = 3$; data not shown). Consistent with Scheme 1, the results of these experiments indicate that transitions between states R and RB (Scheme 1) do not occur at an appreciable rate in either direction under the conditions of our experiments. These sets of experiments confirm several predictions of the trapping model of open channel block.

The previous experiments established that the NMDA-activated channel can close on NEFA and that the receptor can subsequently release agonists. To further investigate the transitions among inhibited states a protocol similar to that shown in Fig. 4 was used, but instead of allowing the amount of antagonism to reach steady state, NEFA was applied for a variable period of time. Following application of antagonist + agonists, the cell was bathed in control solution for 100 s and then agonists were reapplied. This

duration of exposure to control solution was chosen to ensure that all NMDA receptors had sufficient time either to enter the trapped state (RB) or to unbind antagonist and agonists. This protocol allowed us to measure the occupation of state RB as a function of the duration of antagonist application. The data provide insight into the kinetics of the transitions among the closed, blocked states of the channel and were important for evaluation of computational models (see below). In contrast to the steady state experiments, the percent trap observed with brief applications of antagonist was much smaller than the percent block (Fig. 5 A). Both the percent block and percent trap were characterized as a function of the duration of blocker application (Fig. 5 B). The percent inhibition proceeded with a time constant of 10.2 s and reached a steady state value of 96 $\pm$ 0.8%, consistent with Figs. 3 B and 4 A. The percent trap progressed with a similar time constant (13.0 s) and reached a steady state value of 86 $\pm$ 1.7%, consistent with Fig. 4 C.

Single-channel analysis

One of the goals of the research reported here is to develop a quantitative kinetic model of the mechanism of action of NEFA. It is crucial in the development of kinetic models to constrain as many rate constants as possible. We next estimated the values of two rate constants that appear in Scheme 1 using single-channel analysis.

Outside-out patches were exposed to 10 μM NMDA + 10 μM glycine and patch current was recorded, typically for 15 min. Closed and open time histograms and mean burst duration were measured as described in the Methods section. We found that the closed time distribution was adequately fitted by three exponentials (Antonov and Johnson, 1996). The time constants of the three exponentials were 0.61 $\pm$ 0.06 ms, 24.3 $\pm$ 6.2 ms, and 362 $\pm$ 36 ms ($n = 7$). We estimated the rate of channel closure (α in Scheme 1) as the inverse of the mean burst duration (see Methods). The mean value of the burst duration was 8.27 $\pm$ 0.95 ms, corresponding to an α of 121 s^{-1}.
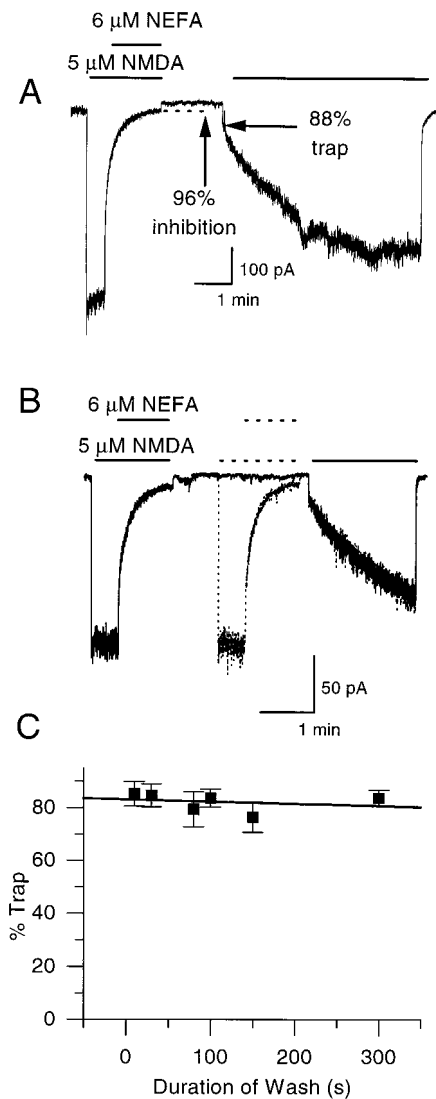
FIGURE 4   NEFA can be trapped within the closed channel. (*A*) After response inhibition reached steady state, both antagonist and agonists were removed. The cell was bathed for 100 s in control solution, and agonists were then reapplied. The response was still substantially antagonized, consistent with the idea that NEFA was trapped within the closed channel. The holding potential was -66 mV. (*B*) NEFA unbinds very slowly or not at all from the closed NMDA channel. Two current traces from the same cell are shown. The current trace drawn with a dotted line begins 120 s later than does the current trace drawn with a solid line. This transposition was performed so that the times of reapplication of agonists can be superimposed. Between application of antagonist + agonists and subsequent application of agonists alone, the cell was washed with control solution for either 150 s (*solid line*) or 10 s (*dotted line*). The two current traces recorded during reapplication of agonists overlay, indicating that NEFA did not escape from the closed channel during the wash with control solution. The holding potential was -66 mV. (*C*) Population data show that there is no correlation between the duration of the wash with control solution and the percent trap ($P > 0.65$).

The forward blocking rate for NEFA (k_+) also was obtained from analysis of single-channel recordings. The value of k_+ can be estimated from the blocker concentration-dependent reduction in either the mean open time or the
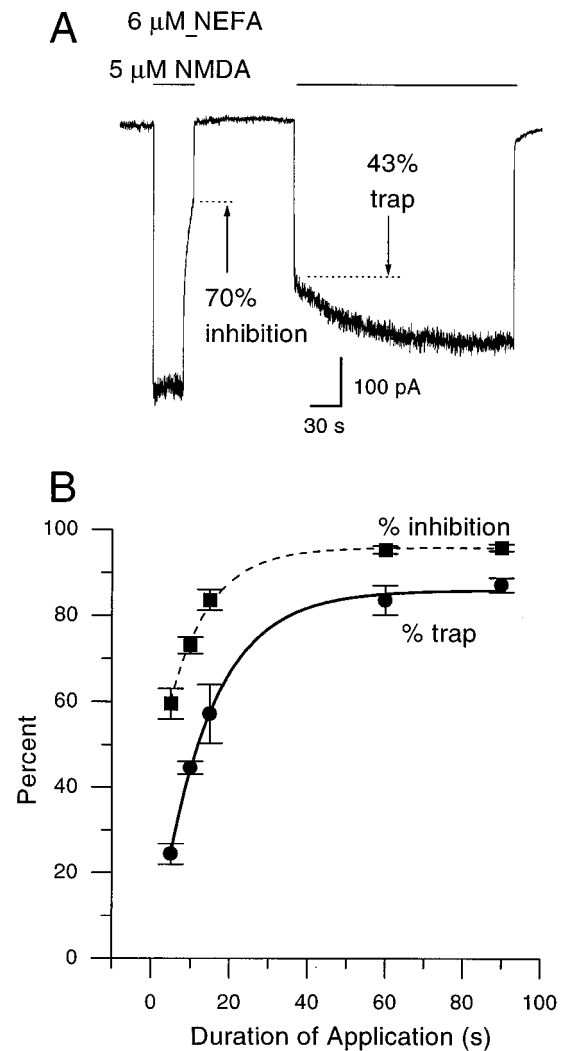

FIGURE 5   Channels accumulate slowly in the trapped state. (*A*) The 10-s application of NEFA is followed by 100 s of wash with Ringer's solution. The percentage of channels that are inhibited at the end of the application of NEFA (*70% inhibition*) is much larger than the percentage of channels that trap antagonist (*43% trap*). The holding potential was -66 mV. (*B*) Percent inhibition and percent trap depend on the duration of the blocker application. The time constant of block is 10.2 s and the steady state value is 96%. Trap proceeds with a time constant of 13.0 s and the steady state value is 86%.

burst duration. Analyzing the mean open time provides a more accurate estimate, especially when data contain a relatively small number of channel openings. The number of channel openings that could be recorded was limited in the presence of high concentrations of antagonist because the blocker greatly reduces the frequency of channel openings. Therefore, we used the reduction in the mean open time to estimate k_+. The mean open time histograms were fitted with one or, more commonly, two exponentials (see Methods). The area of the exponential with the longer time constant was consistently larger, and was used here for estimating k_+.

An open-channel blocker decreases mean open time of a channel according to the equation:

$$\frac{1}{\tau_{o,b}} = \frac{1}{\tau_{o,c}} + k_+[B] \qquad (3)$$

where $\tau_{o,b}$ is the mean open time in the presence of antagonist and agonists, [B] is blocker concentration, $\tau_{o,c}$ is the mean open time under control conditions, and k_+ is the forward rate constant of block (Neher and Steinbach, 1978). NEFA decreased the mean open time in a concentration-dependent manner (Fig. 6). As shown in Fig. 6 *D*, the inverse of τ_o depended linearly on blocker concentration with a slope of 39.9 μM^{-1} s^{-1}. In accord with Eq. 3, this value was used as an estimate of the k_+ of NEFA.

Computational modeling

We next evaluated the hypothesis that NEFA influences receptor operation (e.g., channel gating) while bound within the channel of the NMDA receptor. Because the transitions among blocked states (lower arm of Scheme 1) are electrophysiologically indistinguishable, we used a computational model of Scheme 1 to test the hypothesis. Using the values of rate constants derived from previous work and from the above single-channel analysis (see Methods and Table 1), we fitted Scheme 1 to whole-cell currents recorded in the presence of NEFA and agonists. Hypotheses concerning the effects of blocker binding on specific receptor state transitions were tested by permitting the appropriate rate constants to vary during fitting, as described below.

The model was fitted to five applications (three cells) of 5 μM NMDA + 10 μM glycine and either 2 or 6 μM NEFA recorded at −66 mV. To constrain both the blocking and trapping behavior of the model, "trapping" protocols (protocol shown in Fig. 4) were used for fitting. Only protocols in which the duration of exposure to antagonist was 60 or 90 s and the duration of the subsequent wash with NMDA + glycine was at least 120 s were used.

We first tested the simple hypothesis that receptor operation is not altered by binding of NEFA ("no effect" model). To realize this hypothesis computationally, the values of rate constants in the lower arm were held constant at values equal to the corresponding rate constants in the upper arm of Scheme 1 (Table 1). The only rate constant that was permitted to vary during fitting was the antagonist unbinding rate, k_-. This version of the model provided poor fits to the

FIGURE 6   NEFA causes a reduction in the mean open time of the NMDA channel. (*Left*) Representative single-channel currents from an outside-out patch in the absence (*A*) and the presence of 6 μM (*B*) and 15 μM (*C*) antagonist. The holding potential was −66 mV. (*Right*) The open time histograms for patches exposed to NEFA showed a concentration-dependent reduction in the mean open time. Single channel current and histograms shown in A, B, and C are taken from the same patch. The histogram in A contains 3910 channel openings and was fitted with a double exponential function with time constants (relative areas) of 1.14 ms (0.264) and 5.49 ms (0.736). The histogram in B contains 358 channel openings and was fitted with a double exponential function with time constants (relative areas) of 0.298 ms (0.309) and 2.433 ms (0.691). The histogram in C contains 818 channel openings and was fitted with a single exponential function with a time constant of 1.37 ms. (*D*) NEFA reduces the mean open time of NMDA-activated channels. The mean duration of the prominent mean open time at −66 mV is plotted as a function of concentration of NEFA. Each point represents the mean of three to nine experiments. The slope of the line is the forward rate of antagonism, k_+, and is equal to 39.9 μM^{-1} s^{-1}. The inverse of the intercept is the duration of the prominent mean open time of the unblocked receptor (5.1 ms).
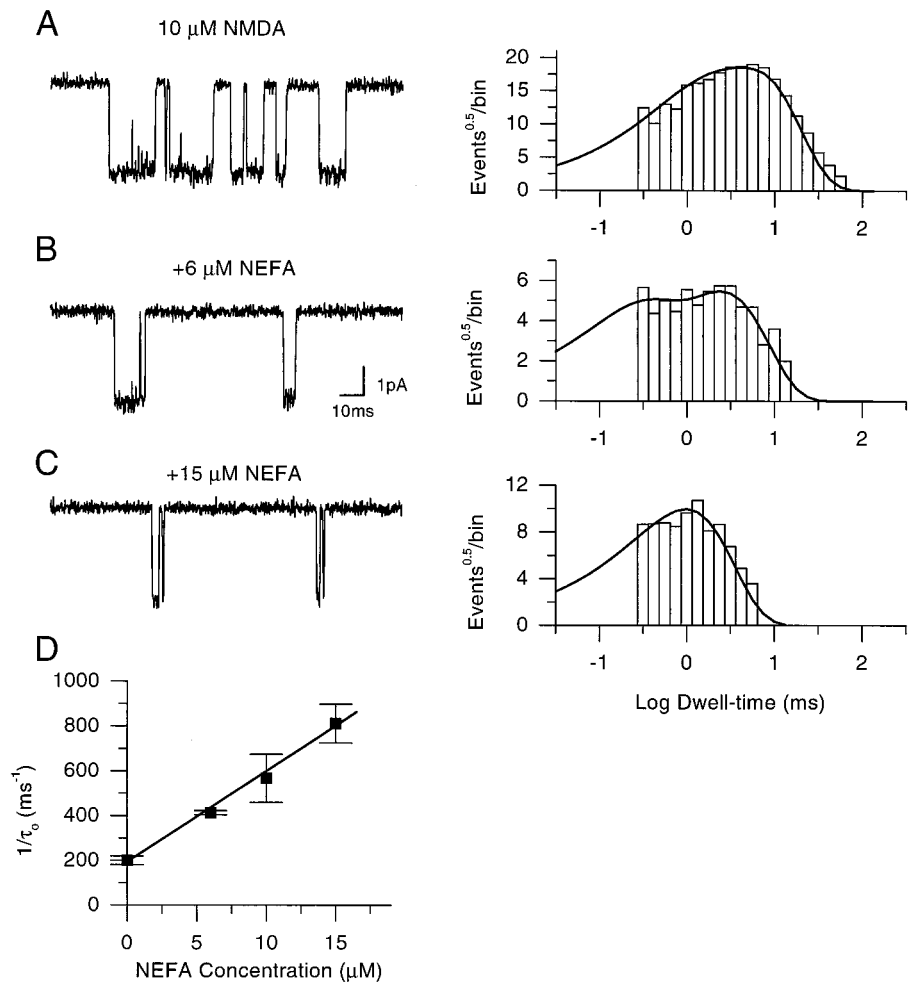
experimental data ($n = 5$; Fig. 7 A), with the inhibition proceeding much more quickly than was experimentally observed.

We next investigated models in which NEFA affects receptor operation. In preliminary fits, we permitted all rate constants in the lower arm of the model to vary. Although this approach provided excellent fits, we found that fits of nearly equal quality could be achieved with widely varying combinations of parameters. We concluded that the model had too many free kinetic parameters (a total of 7) to provide useful testing of hypotheses. Therefore, we re-

FIGURE 7 Fits of the trapping model of channel block to whole-cell recordings of inhibition by NEFA. Whole-cell current (holding potential = −66 mV) is shown with dots; fits of the indicated versions of the trapping model of open channel block (Scheme 1) are shown with solid lines. An application protocol similar to that shown in Fig. 4 was used for model fitting. (A) A poor fit results when it is assumed that NEFA does not affect channel operation (the no effect model). In this model, the only rate constant that was allowed to vary was k_-. (B) By allowing α' and β' (gating model) to vary in addition to k_-, the model fit the data accurately. (C) By allowing k_{a+}' and k_{a-}' (binding model) to vary in addition to k_-, the model again fit the data accurately.

stricted our fitting to two intuitively appealing limiting hypotheses: that NEFA affects exclusively channel opening and closing ("gating" model), or that NEFA affects exclusively agonist binding and unbinding ("binding" model). The gating model was implemented by allowing k_-, α', and β' to vary during fitting runs. Using this model, the model provided excellent fits to the data ($n = 5$; Fig. 7 B). Channel gating is predicted to be slowed considerably when compared to the corresponding transitions in the upper arm of the model. The channel opening rate was slowed 13.4-fold, while the channel closing rate was slowed 2.9-fold. These changes caused an alteration in the maximal probability that a channel is open from 0.025 for unblocked channels to 0.0055 for blocked channels. The binding model (where k_-, k_{a+}', and k_{a-}' were allowed to vary) also provided excellent fits to the data ($n = 5$; Fig. 7 C; Table 1). The agonist unbinding rate was predicted to increase by a factor of 1.3 compared to the corresponding rate for unblocked channels, while the agonist binding rate was reduced 3.5-fold. These values result in a change in the NMDA dissociation constant of each binding site on the receptor from 10.9 μM for unblocked channels to 51.7 μM for blocked channels.

We used two additional approaches to evaluate the validity of these models. First, we used the χ^2 measure of goodness of fit to compare how well each model fit whole-cell current data. The χ^2 for the fits based on the gating and binding models were consistently much lower than the χ^2 for the model which incorporated no change in receptor operation (analysis of variance; $F = 129.54$; $P < 0.001$). The χ^2 from the gating and binding fits were not significantly different from one another, though a trend existed with the gating model producing slightly better fits ($P = 0.020$; 2-tailed t-test with Bonferroni correction; $\alpha_{PW} = 0.01$).

We further tested the validity of each model (the no effect, gating, and binding models) by examining their ability to predict characteristics of NEFA action that were not revealed in the whole-cell experiments to which the models were fit. Each model was used to simulate responses to applications of NEFA + agonists over a wide range of conditions. To permit appraisal of the significance of any discrepancies between model predictions and data, five parameter sets for each model were used. The kinetic parameters in each of the five sets were fixed at the values that provided the best fit to each of the five drug application protocols (see above) to which the model was fit. The five kinetic parameter sets for each of the three models were used to simulate two additional types of protocols.

The first type of protocol simulated with the models was a long application of 0.1 to 10 μM NEFA in the presence of agonists like that shown in Fig. 2 A. The percent antagonism for each simulated current was measured. The individual data points were averaged and are presented as mean ± SE in Fig. 8 A. Both the gating and binding models predict concentration-inhibition curves that are in reasonable agreement with the experimental data. However, the no effect model performed poorly. We next analyzed the kinetics of
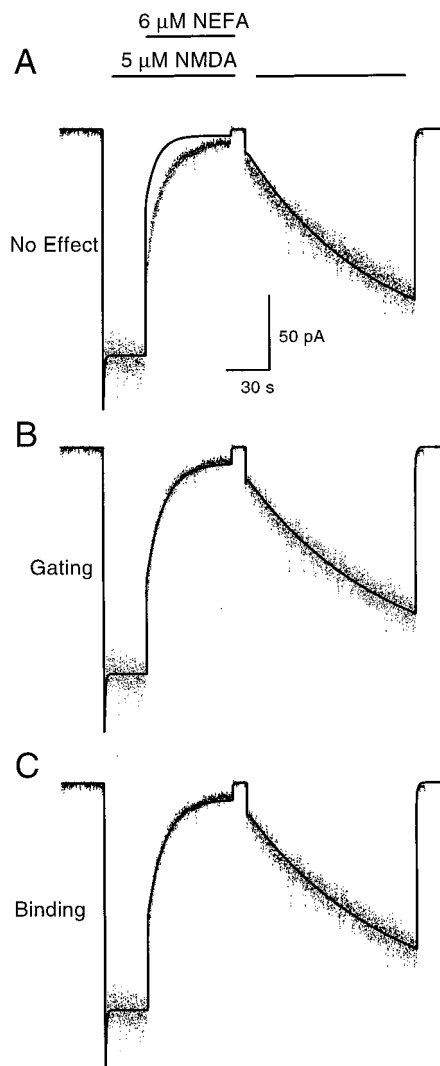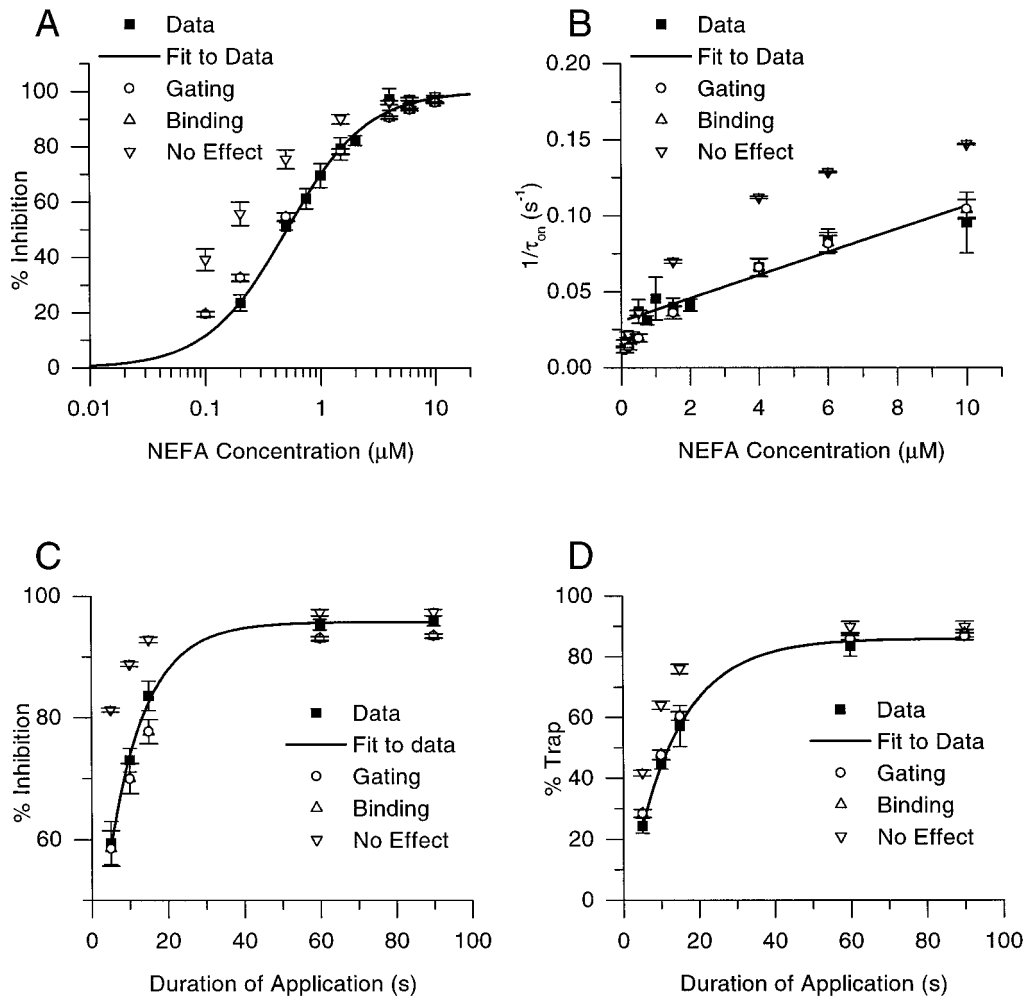
FIGURE 8   Experimentally measured characteristics of inhibition by NEFA compared to predictions of three versions of the trapping model of open channel block. (A) Measured and simulated concentration-inhibition relation for NEFA. Fit of Eq. 1 to experimental data is shown (*solid line*). The IC_{50} and Hill coefficient for each data set are tabulated in Table 2. (B) Measured and simulated dependence on NEFA concentration of the inverse of the time constant of the onset of block. Fit to experimental data is shown (*solid line*). (C, D) Measured and simulated dependence of inhibition (C) and trap (D) on duration of application of 6 μM NEFA. Percent inhibition and percent trap were measured as described in text. Experimental data and single exponential fits (*solid lines*) are replotted from Fig. 5 B. In all plots, the gating and binding model simulations predicted accurately the experimental data while the no effect model produced far less accurate predictions. All data are shown as means ± SE; each simulated data point is the mean of results from five separate simulations (see text).

the simulated currents. For all strategies, the onset and offset of inhibition were multiexponential. To characterize the kinetics of antagonism for comparison to experimental data, simulated current relaxations were fit with single exponential functions. The time constant of the onset of inhibition of predicted currents are plotted against NEFA concentration in Fig. 8 B. The time constants measured from the simulated data employing the gating and binding models were again within the SE of experimental data at most concentrations. In contrast, the simulated data generated by the no effect model were in clear disagreement with experimental data (Fig. 8 B).

The second type of protocol that we used to compare the simulations to experimental data was a trapping protocol similar to that shown in Fig. 5 A. The simulations were comprised of a 15-s application of agonists, an application

of NEFA lasting 5, 10, 15, 60, or 90 s, and a 100-s wash with control solution. Percent inhibition was calculated from the whole-cell current measured just before the removal of NEFA. Percent trap was calculated from the whole-cell current measured just after reapplication of the agonist solution. Again, the gating and binding models performed well in capturing most aspects of the data, including the slow progression of channels into the trapped state. The no effect model again deviated considerably from experimental data points (Figs. 8, C and D). A summary of the performance of the simulations is displayed in Table 2. Based on these data, we reject the no effect model.

Across this variety of test protocols, all of which involved application of 5 μM NMDA, the performance of the binding and gating models was essentially indistinguishable (Figs. 7, 8). However, we found that the predictions of the two
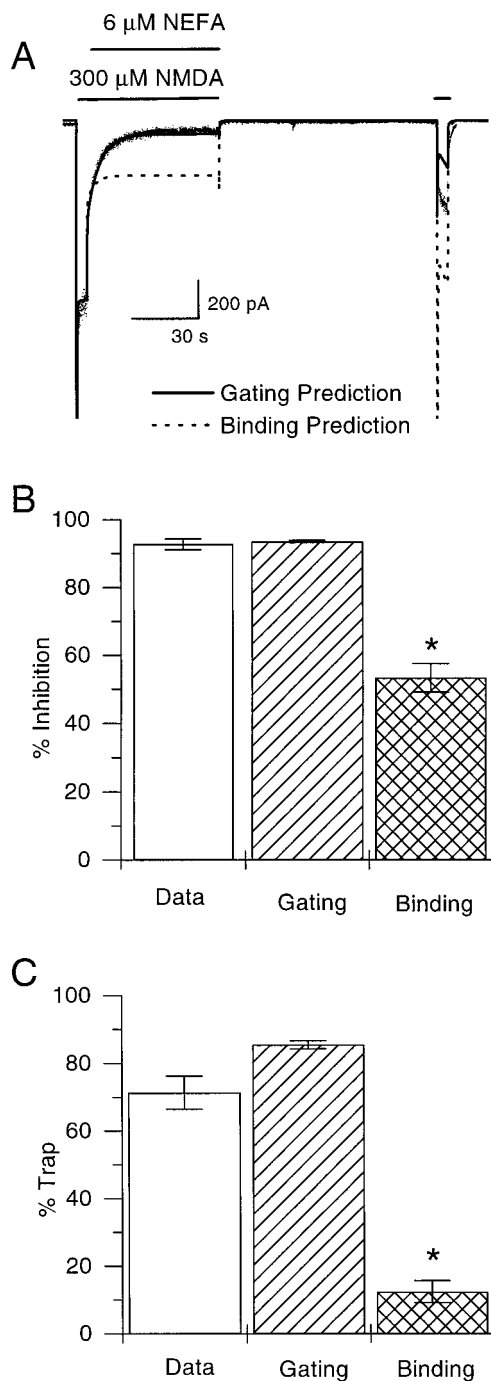
FIGURE 9 The predictions of the gating and binding models differ at high agonist concentration. (*A*) Comparison of whole-cell current (*dots*) and predicted currents derived from the gating (*solid line*) and binding (*dashed line*) models during the indicated applications of 6 μM NEFA and 300 μM NMDA. Holding potential was −66 mV. The simulations were made with no free kinetic parameters; all kinetic parameters were fixed at the average values (Table 2) determined from fits of the gating or binding model to responses in the presence of 5 μM NMDA such as those in Fig. 7. The only parameters allowed to vary during simulation were the number of channels and the baseline current. The models overestimated the amount of desensitization; peak inward currents predicted by both models following the first NMDA application, and by the binding model following the second NMDA application, are truncated. (*B*) Comparison of the percent inhibition measured experimentally (92.7 ± 1.6%; $n = 11$) and predicted by the gating model (93.5 ± 0.3%) and the binding model (53.3 ± 4.2%).

models differ significantly when a higher NMDA concentration was used: the binding model predicts a much stronger dependence of blocker action on agonist concentration than does the gating model. We simulated whole-cell currents according to a trapping protocol similar to that shown in Fig 4 *A* using 300 μM NMDA. Kinetic rate constants derived from fits to applications in 5 μM NMDA and NEFA were used and no kinetic parameters were allowed to vary in creating simulations in 300 μM NMDA. After an application of 6 μM NEFA reached steady state, both antagonist and agonists were removed, the cell was perfused for 100 s with control solution, and agonists were reapplied without antagonist (Fig. 9 *A*). The gating model predicts the percent inhibition and percent trap much more accurately than the binding model (Fig. 9, *B* and *C*).

The data presented above argue strongly that binding of NEFA in the channel of the NMDA receptor affects NMDA receptor operation and that the predominant effect is on channel gating. However, a final concern regarding this conclusion must be addressed. In the no effect model the number of adjustable rate constants is two fewer than in the gating model. The poor performance of the no effect model therefore might be due to an inability to compensate for any inaccuracies in the fixed values of the rate constants in the upper arm of Scheme 1 (see Methods). To address this concern, fits were performed with a "modified no effect" model. In this model the rate constants of the lower arm were fixed to the same value as the corresponding rate constant in the upper arm, but each pair was allowed to vary in unison. Thus, k_-, k_{a+} and k'_{a+}, β and β', k_d and k'_d, k_r and k'_r, and k_{a-} and k'_{a-} were free. Only the parameters directly measured in this study, channel closing rates α and α' and the forward rate of antagonism k_+, were fixed. The modified no effect model possessed three more free parameters than the gating or binding models yet provided poorer fits than those models based on χ^2 estimates of goodness of fit ($P < 0.01$). These results further support the conclusion that NMDA receptor channel gating is affected by the binding of NEFA.

DISCUSSION

In this study we have investigated the interaction between a PCP analog (NEFA) and the NMDA receptor. Electrophysiological experiments were used to characterize the basic inhibitory properties of NEFA. Through computational modeling we demonstrated that a simple model of trapping channel block is able to reproduce and predict many of the

The difference between data and the gating model is not significant ($P > 0.75$); the difference between data and the binding model is significant ($P < 0.001$). (*C*) Comparison of the percent trap measured experimentally (71.5 ± 4.9%; $n = 11$) and predicted by the gating model (85.5 ± 1.2%) and the binding model (12.4 ± 3.3%). The difference between data and the gating model is not significant ($P > 0.09$); the difference between data and the binding model is significant ($P < 0.001$).

characteristics of the inhibition by NEFA. The results of computational modeling suggest that while bound, NEFA influences channel gating in addition to blocking current flow. Both the kinetic and the steady state properties of inhibition by NEFA depend on its ability to influence channel gating.

Pharmacological characteristics

NEFA is an intermediate affinity antagonist of the NMDA receptor (IC_{50} = 0.51 μM). The degree of inhibition was strongly voltage-dependent, suggesting that the binding site for the antagonist is within the channel. NEFA reduced the mean open time of channels in outside out patches in a concentration dependent manner (Fig. 6) with a microscopic binding rate of 39.9 $\mu M^{-1} s^{-1}$. This value is similar to most previous estimates of the microscopic k_+ for other organic channel blockers of the NMDA receptor measured at a similar membrane potential, including 9-aminoacridine (22 $\mu M^{-1} s^{-1}$, Costa and Albuquerque, 1994), arcaine (44 $\mu M^{-1} s^{-1}$, Donevan et al., 1992), the IEM compounds, (12–36 $\mu M^{-1} s^{-1}$, Antonov and Johnson, 1996), MK-801 (30 $\mu M^{-1} s^{-1}$, Huettner and Bean, 1988; 23.7 $\mu M^{-1} s^{-1}$, Jahr, 1992), memantine (31 $\mu M^{-1} s^{-1}$, Blanpied and Johnson, 1995), and amantadine (36.8 $\mu M^{-1} s^{-1}$, Blanpied and Johnson, manuscript in preparation). We conclude that NEFA, like PCP, is a channel blocker of the NMDA receptor.

The mechanism of action of NEFA was investigated at the whole-cell level and was shown to be consistent with the trapping model of open channel block (Scheme 1). NEFA can bind to the open NMDA-activated channel, and be trapped in the channel by closure of the channel gate and agonist dissociation (Fig. 4). In contrast to memantine and amantadine (Blanpied et al., 1997), applications of high concentrations of NEFA (40 μM) in the absence of agonists did not produce inhibition of subsequent responses to NMDA + glycine (data not shown). Although the characteristics of inhibition by NEFA reported here suggest that its mechanism of action is very similar to that of its parent compound, PCP, two principal differences can be noted. First, previous electrophysiological measurements of the affinity of PCP generally (Lerma et al., 1991; MacDonald et al., 1991; but see Parsons et al., 1995) are consistent with the conclusion based on binding measurements (Kozikowski and Pang, 1990) that NEFA is of considerably lower affinity than PCP. Second, NEFA displays the property of "partial trapping;" in 5 μM NMDA, 6 μM NEFA inhibited 96% of the receptors at steady state, whereas 87% of the receptors trapped the drug (Fig. 5 *B*). This situation contrasts with the observation that PCP is trapped by essentially all blocked receptors after simultaneous removal of agonist and antagonist solutions (Lerma et al., 1991). Partial trapping has been also reported for memantine (Blanpied et al., 1997).

Computational modeling

To determine whether binding of NEFA affects NMDA receptor operation, computational modeling of the receptor-blocker interaction was performed. The model of NMDA receptor function (upper arm of Scheme 1) has been used extensively in previous whole-cell studies from several labs (see Methods). While this model reproduces well the properties of whole-cell NMDA-activated currents, reproduction of many of the NMDA receptor properties described in single-channel studies (see, e.g., Gibb and Colquhoun, 1992; Kleckner and Palotta, 1995) would require a far more complex model. There is insufficient information at present to determine the form that such a model should take, nor are there data that would permit constraints on many of the additional required rate constants. Scheme 1 reproduced with surprising accuracy the whole-cell currents measured for this study. Even this simple model contains a number of rate constants that could be determined only by performing fits with free parameters. We therefore decided that use of a more complicated model was not warranted. To limit as far a possible the number of free parameters during fits, we used single-channel recording to measure directly the channel closure rate (α) and the antagonist binding rate (k_+).

Computational modeling of the inhibitory action of NEFA generated significant insights into the interaction between the blocker molecule and the NMDA receptor. In order to constrain the models, we evaluated three limiting hypotheses regarding changes in receptor operation induced by binding of NEFA: binding of NEFA has no effect (no effect model); it alters only channel gating (gating model); or it alters only agonist binding and unbinding (binding model). The gating and binding models made nearly identical predictions when block occurred in a low concentration of NMDA (5 μM). The gating and the binding models' accurate simulation of the accumulation of channels in the trapped state (Fig. 8 *D*) is noteworthy because the models were not fitted to brief applications of NEFA. The gating model proved clearly superior to the binding model, however, in its ability to predict both the inhibition by and trap of NEFA in the presence of 300 μM NMDA (Fig. 9). These divergent predictions result from the 4.8-fold difference between these models in the affinity for NMDA of the receptor with its channel blocked. The kinetic parameters in all models were determined using data sets collected using 5 μM NMDA, and no kinetic parameters were allowed to vary in predicting 300-μM NMDA data. The accurate prediction by the gating model of data measured in 300 μM NMDA is therefore a particularly significant validation of the model. While the data strongly suggest that NEFA affects receptor operation predominantly through an effect on channel gating, a weaker effect on agonist binding cannot be ruled out.

A number of other types of NMDA receptor channel blockers with structures unrelated to PCP have also been shown to influence channel gating. The IEM compounds (Antonov and Johnson, 1996) and 9-aminoacridine (Costa

and Albuquerque, 1994; Benveniste and Mayer, 1995) dras-
tically inhibit channel closure while bound. Amantadine and
memantine also appear to influence channel gating (Blan-
pied et al., 1997; Chen and Lipton, 1997; Blanpied and
Johnson, in preparation), although less strongly than the
IEM compounds or 9-aminoacridine.

Relation between macroscopic and microscopic kinetics

Fig. 3 *B* plots the dependence on blocker concentration of
the macroscopic time constants τ_{on} and τ_{off}, a plot that is
often used in electrophysiological studies of channel block-
ers (e.g., Parsons et al., 1993; Svensson et al., 1994; Chen
and Lipton, 1997). These plots are sometimes used to define
macroscopic rates of block and unblock. While the corre-
spondence between microscopic and macroscopic rates is
straightforward with true noncompetitive or competitive
antagonists, interpretation of macroscopic rates is more
difficult with channel blockers (see, e.g., Parsons et al.,
1995). Using the data and model developed in this paper, we
will evaluate the utility and limitations of the macroscopic
kinetic measurements made here and examine the implica-
tions for related previous studies.

Under conditions in which blocker inhibition kinetics are
in the seconds range or slower, it is often assumed that
antagonist binding and unbinding are rate-limiting steps
(e.g., Huettner and Bean, 1988; MacDonald et al., 1991). If
this rate-limiting assumption is correct, then explicit equa-
tions can be used to relate macroscopic current relaxations
and microscopic receptor properties. The rate-limiting as-
sumption implies that the relative occupancy of each state in
the upper arm of Scheme 1 remains approximately at equi-
librium levels (the arm is in pseudo-equilibrium) during
block and unblock. The same would apply to relative occu-
pancies of states in the lower arm of the model. If the rate
limiting hypothesis were correct, the current relaxation fol-
lowing antagonist concentration jumps such as those shown
in Fig. 3 *A* would be single exponential. For channel block-
ers that follow Scheme 1, the time constant of the current
relaxation following a jump into blocker (τ_{on}) would
depend on blocker concentration according to the following
expression:

$$1/\tau_{on} = k_+ \cdot [\text{B}] \cdot P_{open|unblocked} + k_- \cdot P_{open|blocked} \quad (4)$$

where $P_{open|unblocked}$ is the conditional probability that a
channel is open given that it is unblocked and $P_{open|blocked}$ is
the conditional probability that a channel is open given that
it is blocked. The relation between $1/\tau_{on}$ and [B] would be
linear with a slope (sometimes called the macroscopic
blocking rate) of $P_{open|unblocked} \cdot k_+$.

If reasonably accurate, Eq. 4 would permit simple inter-
pretation of macroscopic rates of channel blockers. Using
the experimental data and gating model developed here, we
can evaluate the validity of the rate-limiting assumption and
Eq. 4 for NEFA (Fig. 10). The fractional occupancies of

states R^*A_2 and R^*A_2B are shown in Fig. 10 *B*. Fractional
occupancy is defined as the fractional of all receptors that
are in the indicated state. The conditional probability
$P_{open|unblocked}$ is defined as the occupancy of state R^*A_2
(Fig. 10 *B*) divided by the occupancy of all states without
blocker bound (R, RA, RA_2, R_d and R^*A_2). Similarly,
$P_{open|blocked}$ is the occupancy of R^*A_2B (Fig. 10 *B*) divided
by the occupancy of all states with blocker bound (RB,
RAB, RA_2B, R_dB, and R^*A_2B). If the rate-limiting assump-
tion is correct, then $P_{open|unblocked}$ and $P_{open|blocked}$ should
remain constant (pseudo-equilibrium should be maintained)
during periods when the concentrations of agonists and
NEFA remain constant. It is clear from Fig. 10 *C (left)* that
this prediction is incorrect at a low agonist concentration.
When a high agonist concentration is used (Fig. 10 *C, right*),
the kinetics of agonist action are faster but pseudo-equilib-
rium is still not approached. Note that, although kinetics of
block are faster in higher agonist concentration, there still is
a slow component of channel block (Fig. 10 *A, right*). None
of the slow current relaxations shown in Fig. 10 *A* can be
explained by any of the rate constants in the model (Table
1). Instead, the slow macroscopic time constants result from
the combined effects of low occupancy of open states (Fig.
10 *C*) and microscopic rates of block or unblock.

The quantitative consequences of the lack of pseudo-
equilibrium demonstrated in Fig. 10 *C* can be assessed
using Eq. 4. This equation could be used to calculate
$P_{open|unblocked}$ with any channel blocker if the rate limiting
assumption were correct. In the case of 5 μM NEFA, the
slope of a line fit to the data shown in Fig. 3 *B* is 0.0097
μM^{-1} s^{-1} (Table 2); dividing by $k_+ \cdot \beta$ (Eq. 4) yields an
estimate of $2.4 \cdot 10^{-4}$ for $P_{open|unblocked}$. However, the true
value of $P_{open|unblocked}$ in the gating model under these
conditions is $1.6 \cdot 10^{-3}$ (Fig. 10 *C*). Thus, the quantitative
inaccuracies associated with incorrectly making the rate-
limiting assumption can be substantial.

One experimental implication of these conclusions con-
cerns block by MK-801. The macroscopic unbinding rate of
MK-801 is so slow that inhibition may be considered irre-
versible over the time course of most electrophysiological
experiments. The assumption that this reflects an extremely
slow microscopic k_- of MK-801 has been essential for
estimates of the value of $P_{open|unblocked}$ (Huettner and Bean,
1988; Jahr, 1992; Rosenmund et al., 1995). However, com-
parison of the microscopic rate constants and macroscopic
kinetics of the models developed here reveals that even
gross estimates of microscopic rate constants should not be
based on macroscopic kinetics. When a channel binds
blocker, it enters state R^*A_2B, the mean lifetime of which is
determined by the rates of transition to R^*A_2 (k_-) and to
RA_2B (α'). The transition possessing the faster rate is more
likely to occur. In the gating model presented here, the
channel is *more* likely to unbind NEFA than to close (Table
1). Channels will, on average, rapidly bind and unbind
blocker over two times before closing; k_+ therefore is not
the rate of entry into a state with mean lifetime reflected by
the macroscopic unbinding rate. Although similar kinetic

FIGURE 10 Simulated currents, fractional occupancies, and conditional occupancies of selected states in the gating model. The plots were generated by using the average rate constants from Table 1 with applications of 6 μM NEFA in 5 μM (*left*) and 300 μM NMDA. (*A*) Whole-cell currents were simulated using an agonist and antagonist application protocol similar to that shown in Fig. 4 *A*. The current in 300 μM NMDA is truncated at -800 pA. (*B*) Fractional occupancy of states R^*A_2 and R^*A_2B during application of NMDA and NEFA. The fractional occupancy of R^*A_2 is proportional to the absolute value of current. The occupancy of R^*A_2 in 300 μM NMDA is truncated at 0.005. (*C*) $P_{\text{open|blocked}}$ and $P_{\text{open|unblocked}}$ vary during the application of NEFA. $P_{\text{open|blocked}}$ is undefined and therefore not plotted until NEFA is applied. Note that following application of NEFA, there is a large and sustained change in conditional probabilities.
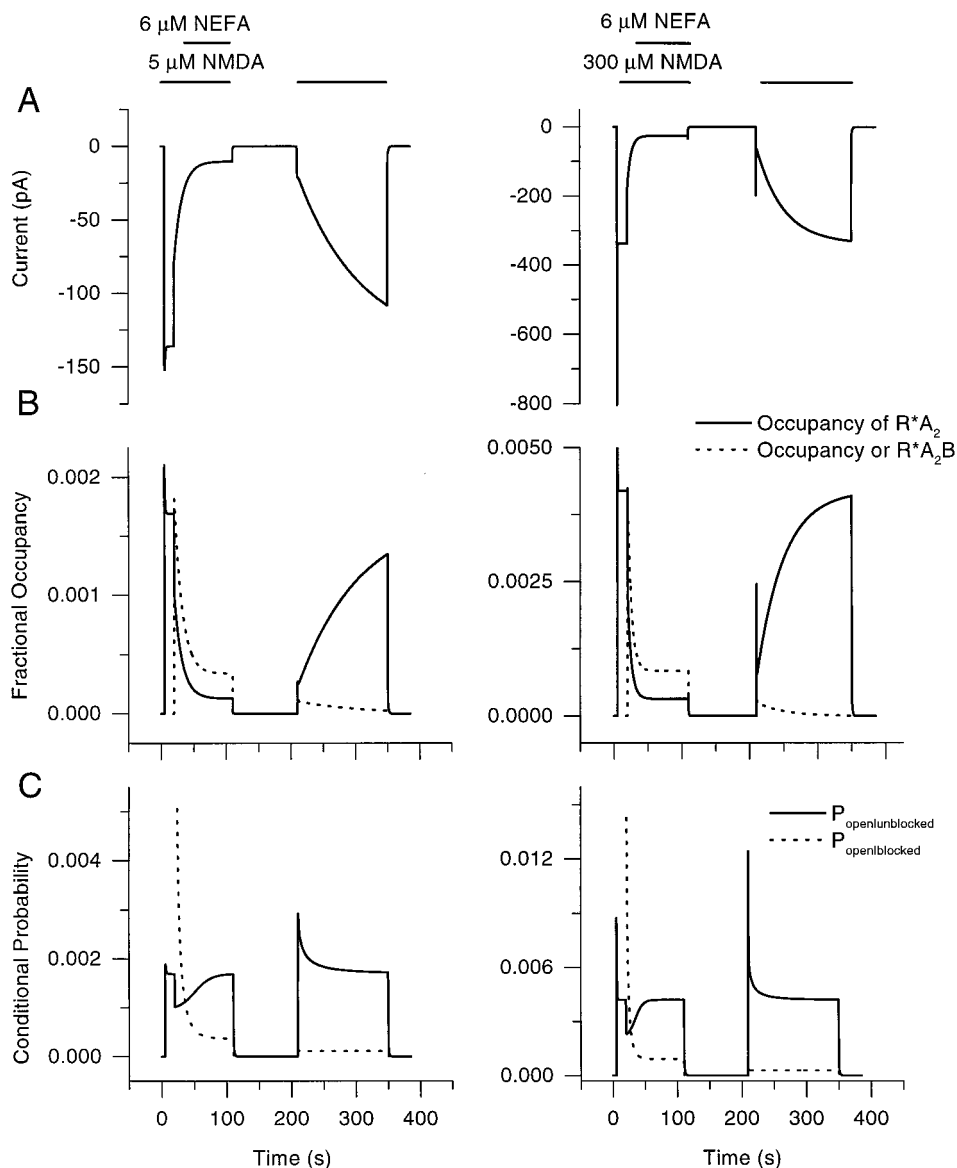
information is not available for MK-801, it too might plausibly block and unblock more than once before a very long-lived blocked state other than R^*A_2B is entered. If this were the case, then k_+ as measured in single-channel experiments would be an overestimate of the rate of entry into a very long-lived state. The value of $P_{\text{open|unblocked}}$ estimated from MK-801 block experiments then would be underestimated. If, for example, MK-801 on average blocks channels two times before the receptor enters a very long-lived blocked state, the estimates of $P_{\text{open|unblocked}}$ will be low by a factor of about 2.

In all cases examined so far, the mechanism of action of channel blockers depends not only on interaction with the open channel but also on the effects of blocker binding on receptor operation (e.g., Armstrong, 1971; Ascher et al., 1978; Neher, 1982; Lingle, 1983; Antonov and Johnson, 1996; Blanpied et al., 1997; this study). The effect of blocker binding on receptor or channel operation can influence profoundly the kinetic and steady state characteristics of antagonism. These characteristics may in turn govern the therapeutic potential of channel blockers of NMDA receptors (Chen et al., 1992; Rogawski, 1993). Similarly, the effects of PCP and related drugs on receptor operation may explain why they are uniquely able to mimic the behavioral effects of schizophrenia. Improved models of blocker-receptor interactions will advance the understanding of the diversity of effects of NMDA receptor channel blockers and the design of new blockers with improved therapeutic utility.

REFERENCES

Adams, P. R. 1976. Drug blockade of open end-plate channels. *J. Physiol. (London).* 260:531–551.

Antonov, S. M., and J. W. Johnson. 1996. Voltage-dependent interaction of open channel blocking molecules with gating of NMDA receptors in rat cortical neurons. *J. Physiol. (London).* 493:425–445.

Antonov, S. M., J. W. Johnson, N. Y. Lukomskaya, N. N. Potapyeva, V. E. Gmiro, and L. G. Magazanik. 1995. Novel adamantane derivatives act as blockers of open ligand-gated channels and as anticonvulsants. *Mol. Pharmacol.* 47:558–567.

Armstrong, C. M. 1971. Interaction of tetraethylammonium ion derivatives with the potassium channels of giant axons. *J. Gen. Physiol.* 58:413–437.

Ascher, P., A. Marty, and T. O. Neild. 1978. The mode of action of antagonists of the excitatory response to acetylcholine in *Aplysia* neurones. *J. Physiol. (London).* 278:207–235.

Benveniste, M., and M. L. Mayer. 1991. Kinetic analysis of antagonist action at N-methyl-D-aspartic acid receptors. *Biophys. J.* 59:560–573.

Benveniste, M., and M. L. Mayer. 1996. Trapping of glutamate and glycine during open channel block of rat hippocampal neuron NMDA receptors by 9-aminoacridine. *J. Physiol. (London).* 483:367–384.

Blanpied, T. A., F. Boeckman, E. Aizenman, and J. W. Johnson. 1997. Trapping channel block of NMDA-activated responses by amantadine and memantine. *J. Neurophysiol.* 77:309–323.

Chen, H. S. V., and S. A. Lipton. 1997. Mechanism of memantine block of NMDA-activated channels in rat retinal ganglion cells: uncompetitive antagonism. *J. Physiol. (London).* 499:27–46.

Chen, H. S. V., J. W. Pellegrini, S. K. Aggarwal, S. Z. Lei, S. Warach, F. E. Jensen, and S. A. Lipton. 1992. Open-channel block of N-methyl-D-aspartate (NMDA) responses by memantine: therapeutic advantage against NMDA receptor-mediated neurotoxicity. *J. Neurosci.* 12:4427–4436.

Clements, J. D., R. A. J. Lester, G. Tong, C. E. Jahr, and G. L. Westbrook. 1992. The time course of glutamate in the synaptic cleft. *Science.* 258:1498–1501.

Clements, J. D., and G. L. Westbrook. 1991. Activation kinetics reveal the number of glutamate and glycine binding sites on the N-methyl-D-aspartate receptor. *Neuron.* 7:605–613.

Clements, J. D., and G. L. Westbrook. 1994. Kinetics of AP5 dissociation from NMDA receptors: Evidence for two identical cooperative binding sites. *J. Neurophysiol.* 71:2566–2569.

Colquhoun, D., and A. G. Hawkes. 1995. Desensitization of N-methyl-D-aspartate receptors: A problem of interpretation. *Proc. Natl. Acad. Sci. USA.* 92:10327–10329.

Colquhoun, D., and F. J. Sigworth. 1995. Fitting and statistical analysis of single-channel records. *In* Single-Channel Recording. B. Sakmann and E. Neher, editors. Plenum Press, New York. 483–585.

Costa, A. C. S., and E. X. Albuquerque. 1994. Dynamics of the actions of tetrahydro-9-aminoacridine and 9-aminoacridine on glutamatergic currents: concentration-jump studies in cultured rat hippocampal neurons. *J. Pharmacol. Exp. Ther.* 268:503–514.

Dilmore, J. G., and J. W. Johnson. 1994. Open channel block of the NMDA activated channel by structural analogue of phencyclidine. *Soc. Neurosci. Abstr.* 20:1141.

Dilmore, J. G., and J. W. Johnson. 1995. Kinetic modeling of the block of open NMDA-activated channels by a structural analogue of phencyclidine. *Soc. Neurosci. Abstr.* 21:352.

Ditzler, K. 1991. Efficacy and tolerability of memantine in patients with dementia syndrome. *Arzneimittel Forschung.* 41:773–780.

Donevan, S. D., S. M. Jones, and M. A. Rogawski. 1992. Arcaine blocks N-methyl-D-aspartate receptor responses by an open channel mechanism: whole-cell and single-channel recording studies in cultured hippocampal neurons. *Mol. Pharmacol.* 41:727–735.

Ellison, G. 1995. The N-methyl-D-aspartate antagonists phencyclidine, ketamine and dizocilpine as both behavioral and anatomical models of the dementias. *Brain Res. Brain Res. Rev.* 20:250–267.

Fischer, P. A., P. Jacobi, E. Schneider, and B. Schönberger. 1977. Effects of intravenous administration of memantine in Parkinson's patients. *Arzneimittel Forschung.* 27:773–780.

Gibb, A. J., and D. Colquhoun, 1992. Activation of NMDA receptors by L-glutamate in cells dissociated from adult rat hippocampus, *J. Physiol. (London).* 456:462–464.

Hamill, O. P., A. Marty, E. Neher, B. Sakmann, and F. J. Sigworth. 1981. Improved patch-clamp techniques for high-resolution current recording from cells and cell-free membrane patches. *Pflügers Arch.* 391:85–100.

Howe, J. R., D. Colquhoun, S. G. Cull-Candy. 1988. On the kinetics of large-conductance glutamate-receptor ion channels in rat cerebellar granule neurons. *Proc. R. Soc. Lond.* 233:407–422.

Huettner, J. E., and B. P. Bean. 1988. Block of N-methyl-D-aspartate-activated current by the anticonvulsant MK-801: selective binding to open channels. *Proc. Natl. Acad. Sci. USA.* 85:1307–1311.

Jahr, C. E. 1992. High probability opening of NMDA receptor channels by L-glutamate. *Science.* 255:470–472.

Jahr, C. E., and C. F. Stevens. 1990. A quantitative description of NMDA receptor-channel kinetic behavior. *J. Neurosci.* 10:1830–1837.

Johnson, J. W., S. M. Antonov, T. A. Blanpied, and Y. Li-Smerin. 1995. Channel block of the NMDA receptor. *In* Excitatory Amino Acids and Synaptic Transmission. H. V. Wheal and A. M. Thomson, editors. Academic Press, San Diego, CA. 99–113.

Johnson, J. W., and P. Ascher. 1990. Voltage-dependent block by intra-cellular Mg^{2+} of N-methyl-D-aspartate-activated channels. *Biophys. J.* 57:1085–1090.

Kleckner, N. W., and B. S. Palotta. 1995. Burst kinetics of single NMDA receptor currents in cell-attached patches from rat brain cortical neurons in culture. *J. Physiol. (London).* 486:411–426.

Kozikowski, A., and Y. Pang. 1990. Structural determinants of affinity for the phencyclidine binding site of the N-methyl-D-aspartate receptor complex: discovery of a rigid phencyclidine analogue of high binding affinity. *Mol. Pharmacol.* 37:352–357.

Krystal, J. H., L. P. Karper, J. P. Seibyl, G. K. Freeman, R. Delaney, J. D. Bremmer, G. R. Heninger, M. J. Bowers, and D. S. Charney. 1994. Subanesthetic effects of the noncompetive NMDA antagonist, ketamine, in humans: psychotomimetic, perceptual, cognitive, and neuroendocrine responses. *Arch. Gen. Psychiatry.* 51:199–214.

Lerma, J., R. S. Zukin, and M. V. L. Bennett. 1991. Interaction of Mg^{2+} and phencyclidine in use-dependent block of NMDA channels. *Neurosci. Lett.* 123:187–91.

Lester, R. A. J., and C. E. Jahr. 1992. NMDA channel behavior depends on agonist affinity. *J. Neurosci.* 12:635–643.

Lester, R. A. J., G. Tong, and C. E. Jahr. 1993. Interactions between the glycine and glutamate binding sites of the NMDA receptor, *J. Neurosci.* 13:1993.

Lingle, C. 1983. Different types of blockade of crustacean acetylcholine-induced currents. *J. Physiol. (London).* 339:419–437.

Luby, E. D., B. D. Cohen, F. Rosenbaum, J. Gottlieb, and R. Kelley. 1959. Study of a new schizophrenomimetic drug. *Arch. Neurol. Psychiatry.* 81:363–369.

MacDonald, J. F., M. C. Bartlett, I. Mody, P. Pahapill, J. N. Reynolds, M. W. Salter, J. H. Schneiderman, and P. S. Pennefather. 1991. Actions of ketamine, phencyclidine and MK-801 on NMDA receptor currents in cultured mouse hippocampal neurones. *J. Physiol. (London).* 432:483–508.

Mayer, M. L., A. B. MacDermott, G. L. Westbrook, S. J. Smith, and J. L. Baker. 1987. Agonist- and voltage-gated calcium entry in cultured mouse spinal cord neurons under voltage clamp measured using Arsenazo III. *J. Neurosci.* 7:3230–3244.

Mayer, M. L., G. L. Westbrook, and L. Vyklický Jr. 1988. Sites of antagonist action on N-methyl-D-aspartic acid receptors studied using fluctuation analysis and a rapid perfusion technique. *J. Neurophysiol.* 60:645–663.

McBain, C. J., and M. L. Mayer. 1994. N-methyl-D-aspartic acid receptor structure and function. *Physiol. Rev.* 74:723–760.

Neher, E. 1982. The charge carried by single-channel currents of rat cultured muscle cells in the presence of local anesthetics. *J. Physiol. (London).* 339:663–678.

Neher, E., and J. H. Steinbach. 1978. Local anaesthetics transiently block currents through single acetylcholine-receptor channels. *J. Physiol. (London).* 277:153–176.

Nowak, L., P. Bregestovski, P. Ascher, A. Herbet, and A. Prochiantz. 1984. Magnesium gates glutamate-activated channels in mouse central neurones. *Nature.* 307:462–465.

Parsons, C. G., R. Gruner, J. Rozental, J. Millar, and D. Lodge. 1993. Patch clamp studies on the kinetics and selectivity of N- methyl-D-aspartate receptor antagonism by memantine (1-amino- 3,5-dimethyladamantan). *Neuropharmacology.* 32:1337–1350.

Parsons, C. G., V. A. Panchenko, V. O. Pinchenko, A. Y. Tsyndrenko, and O. A. Krishtal. 1996. Comparative patch-clamp studies with freshly dissociated rat hippocampal and striatal neurons on the NMDA receptor antagonistic effects of amantadine and memantine. *Eur. J. Neurosci.* 8:446–454.

Rogawski, M. A. 1993. Therapeutic potential of excitatory amino acid antagonists: channel blockers and 2,3-benzodiazepines. *Trends Pharmacol. Sci.* 14:325–331.

Rosenmund, C., A. Feltz, and G. L. Westbrook. 1995. Synaptic NMDA receptor channels have a low open probability. *J. Neurosci.* 15:2788–2795.

Rosenmund, C., and G. L. Westbrook. 1993. Rundown of N-methyl-D-aspartate channels during whole-cell recording in rat hippocampal neurons: role of Ca^{+2} and ATP. *J. Physiol. (London).* 470:705–729.

Rothman, S. M., and J. W. Olney. 1995. Excitotoxicity and the NMDA receptor- still lethal after eight years. *Trends Neurosci.* 18:57–58.

Sather, W., J. W. Johnson, G. Henderson, and P. Ascher. 1990. Glycine-insensitive desensitization of NMDA responses in cultured mouse embryonic neurones. *Neuron.* 4:725–731.

Sigworth, F. J., and S. M. Sine. 1987. Data transformations for improved display and fitting of single-channel dwell time histograms. *Biophys. J.* 52:1047–1054.

Svensson, B. E., T. R. Werkman, and M. A. Rogawski. 1994. Alaproclate effects on voltage-dependent K^+ channels and NMDA receptors: studies in cultured rat hippocampal neurons and fibroblast cells transformed with Kv1.2 K^+ channel cDNA. *Neuropharmacology.* 33:795–804.

Traynelis, S. F., and S. G. Cull-Candy. 1991. Pharmacological properties and H^+ sensitivity of excitatory amino acid receptor channels in rat cerebellar granule neurones. *J. Physiol. (London).* 433:727–763.

Vyklický, L. Jr., M. Benveniste, and M. L. Mayer. 1990. Modulation of N-methyl-D-aspartic acid receptor desensitization by glycine in mouse cultured hippocampal neurones. *J. Physiol. (London).* 428:313–331.

Woodhull, A. M. 1973. Ionic blockage of sodium channels in nerve. *J. Gen. Physiol.* 61:687–708.